PHILOSOPHICAL MAGAZINE
https://doi.org/10.1080/14786435.2025.2450217

Taylor & Francis
Taylor & Francis Group

Check for updates

Compression of a line of spheres or bubbles in a transverse confining potential

J. Ryan-Purcell[a], A. Irannezhad [a], M. Whelan[a], D. Weaire[a], A. Mughal [b] and
Q2 Q1 S. Hutzler[a]

Q3 [a]School of Physics, Trinity College Dublin, The University of Dublin, Ireland; [b]Department of Mathematics, Aberystwyth University, Penglais, Aberystwyth, UK

ABSTRACT
A line of spheres or bubbles, confined in a cylindrically symmetric harmonic potential, buckles under axial compression. Increasing compression results in a sequence of initially planar, and eventually non-planar, structures. We present a catalogue of these, drawing on both experiments and computer simulations. The latter make use of the theory of Morse and Witten to model bubble–bubble interaction. Numerical results are summarised in stability diagrams, of potential relevance to the creation of chiral photonic crystals from self-assembled packings of spheres.

ARTICLE HISTORY
Received 21 August 2024
Accepted 21 December 2024

KEYWORDS
Columnar crystals; sphere packings; soft spheres; self-assembly

1. Introduction

Densely packed cylindrical arrangements of spheres, hard or soft (such as shown in Figures 1 and 2), are found on many length scales [1]. In the teaching laboratory, tennis balls or hydrogel spheres provide for excellent demonstrations [2]. Examples from biology include the familiar arrangements of berries or seeds around a stem ($\sim 10^{-2}$ m), or the structure of the notochord of the zebrafish ($\sim 10^{-5}$ m) [3]. Silica spheres with diameter between several hundred nanometres and a few micrometres can form ordered columnar (colloidal) crystals [4]. Chiral sphere packings (made of either conducting or dielectric materials) are currently being explored for the use in photonics [5], to create crystals which display circular dichroism (different absorption of left- and right-handed circularly polarised light). Of particular relevance to applications is the fact that the ordered packings form by *self-assembly*.

The exploration of chirality is also at the heart of studies of arrangements of Janus particles [6, 7]. These particles may be modelled as consisting of hemispheres with different physico-chemical properties, resulting for example in a hydrophilic and a hydrophobic half. Using molecular dynamics simulations,

CONTACT S. Hutzler shutzler@maths.tcd.ie

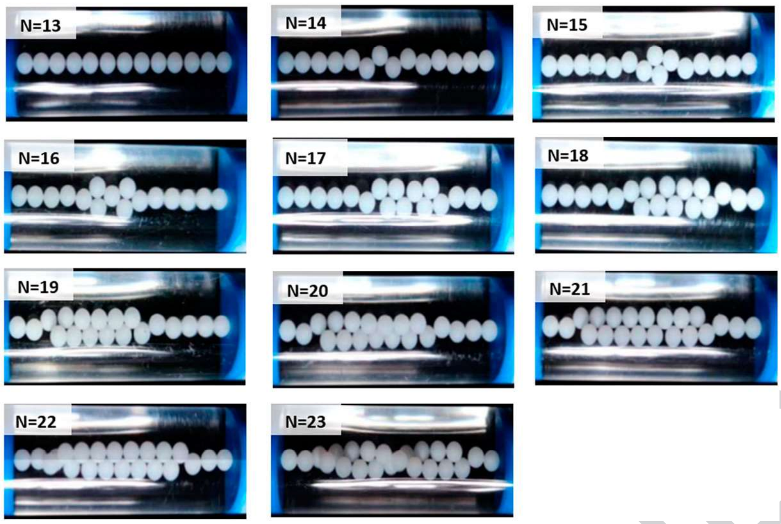

Figure 1. Arrangements of polypropylene spheres confined in a water-filled cylinder, rotating at 1800 rpm, and viewed using a stroboscopic light source. The chain buckles at $N = 14$, and at $N = 15$ a doublet forms. For $N = 16$–22, further contacts are formed, resulting in what we call a *zipper* structure. At $N = 23$ the zipper twists. (Distance between hard walls 40.7 mm, sphere diameter 3 mm.)

Fernández *et al.* [7] studied the helical arrangements of Janus particles placed in a cylindrically symmetric harmonic confining potential. Varying the strength of the electrostatic interaction between the particles, or the packing fraction, resulted in the formation of several different columnar crystals. These included the straight line of particles, a planar zig-zag chain, a planar double chain, a 'rectangular chain', and structures that are made up of two or three intertwined spirals, the Boerdijk–Coxeter helix [8, 9] or Bernal spiral (Bernal having recognised the relevance of Boerdijk's locally dense structure for the structure of liquids [10, 11]). Like many such columnar structures it features in biological contexts (e.g. proteins) [12].

One method for generating a cylindrically symmetric potential is that used in the experiments conducted by Lee *et al.* [13], which inspired contributions from

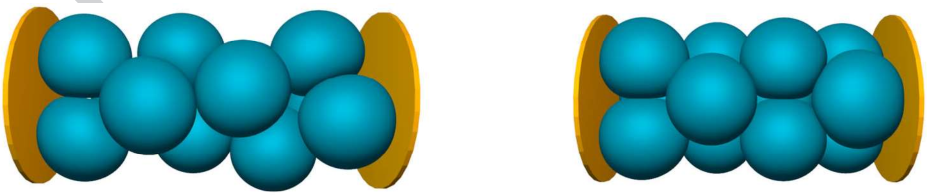

Figure 2. Results of Morse–Witten model simulations of a 12-bubble system for the ratio $k/\gamma = 0.75$. (Left) Boerdijk spiral at length $L/D = 3.75$. (Right) 3-3-0 structure at length $L/D = 3.35$. The bubble shapes are drawn using analytic expressions from the Morse–Witten model; rendering was applied using the software Blender [28].

our research group. Spheres, lighter than water, are immersed into a water-filled cylinder which is spun around its long axis by mounting it horizontally on a lathe. Driven by a centripetal force under a high rate of rotation, the spheres arrange themselves along this axis. Lee *et al.* identified the range of number densities for which particular structures are found and presented this experimental data, together with results from molecular dynamics simulations, in the form of a phase diagram [13]. Some of the reported structures are identical to those seen in the particle simulations by Sobrino Fernandez *et al.* mentioned above [7].

In the following we will describe the sequence of the simplest such structures which form upon compression of an initially straight line of spheres, confined in a transverse harmonic potential, akin to confinement by the centripetal force in the lathe experiment. The progressive buckling of such a line, up to the point of formation of additional contacts (in a so-called *doublet*) was recently described by us using a continuum description [14]. Here we will report computer simulations which go beyond these initial stages, leading to a variety of three-dimensional structures.

Our simulations make use of the theory of Morse and Witten for modelling bubble–bubble interactions [15, 16]. Unlike the simple heuristic model of soft particles as overlapping spheres, this theory is derived from the Laplace–Young equation for bubbles, allowing (in lowest order) for deviations from sphericity in response to bubble–bubble contacts. Results are presented in the form of stability diagrams. By highlighting the role of finite size effects, these diagrams also offer guidance for further experimental or numerical studies.

For illustrative purposes we will in Section 2 present our experimental data obtained for hard spheres placed in a lathe, as in the experiments by Lee *et al.* [13].

2. Experiments with hard spheres contained in a rotating liquid-filled cylinder

Our experiments with hard spheres extend and complement those of [13], in which the confining potential is provided by placing spheres in a water-filled rotating cylinder mounted in a lathe. We are particularly interested in the most simple structures, which are not discussed by [13]. Furthermore, as in our corresponding simulations of Section 3, we use much smaller numbers of spheres and display both cylinder ends to show the role of boundaries. In contrast to the case with a large number of spheres, where boundary effects are minimal, we find that the boundaries stabilise structural variants that would not be observed in long packings with many spheres, where boundary effects are negligible. This results in a much richer variety of packings.

The transparent perspex cylinder, containing N spheres of diameter D, is sealed at both ends with stoppers and mounted horizontally onto a lathe. The spheres (polypropylene beads, density $\rho = 0.900\,\mathrm{g/cm^3}$, diameter $D = 3.0\,\mathrm{mm}$ [17]) are buoyant in water and are thus pushed towards the axis of the cylinder when the latter is rotated (1800 rpm for the examples shown in Figure 1). We keep the distance, L, between the two stoppers fixed in all our experiments, $L = 40.7\,\mathrm{mm}$, but vary the number, N, of spheres that are added to the cylinder before it is sealed and set into rotation. (An alternative procedure would be to keep the number of spheres fixed, and change the cylinder length L, possibly even while the cylinder is rotating. We have not pursued the latter, as it would require a more advanced experimental set-up.)

To observe the structures in steady rotation within the cylinder, we use a stroboscopic light source, with a frequency set to the rotation frequency; the sphere arrangements are then readily captured using standard video imaging. To eliminate transient effects, the cylinder is rotated for at least two minutes before capturing images, ensuring steady-state conditions are reached.

For our values of stopper spacing $L = 40.7$ mm and sphere diameter $D = 3.0$ mm up to $N = 13$ spheres can align along the cylinder axis in a straight line (see Figure 1). For $N = 14$ this is no longer possible. Instead, the spheres form a modulated *zig–zag* arrangement, with the transverse displacement due to buckling being maximal near the centre of the cylinder.

For $N = 15$, we observe what we call a *doublet*; four spheres of the chain have additional contacts. Performing the experiments with more spheres ($15 < N \lesssim 22$) results in several more spheres having three or four contacts; this can occur anywhere along the chain. In some of the observed arrangements the doublets combine to form an extended structure which we call a *zipper* [18]; see the photos for $N = 18$ to 22 in Figure 1 for some examples. The observed zipper structures remain planar up to $N = 22$. For $N = 23$, which is the largest number of spheres that we used in our experiments, the zipper is *twisted*.

3. Computer simulations

In the following we present simulation results for two models which differ in their treatment of bubble–bubble interaction. In the soft sphere model, which was called 'the "Ising model" for jamming' in the seminal review by van Hecke [19], interactions are simple pairwise, with either harmonic or Hertzian forces between contacting bubbles being in use. In the context of foams, the harmonic version is also referred to as Durian's 'Bubble Model' (which may include a viscous drag force [20], not relevant to the static configurations considered here). Despite its simplicity the model allows for the computation of the structures shown in Figure 1. In the physically more realistic Morse–Witten model [15, 16] the interaction between contacting bubbles is nonlinear and non-local. Our simulations using the soft sphere model are described in Section 3.1, Section 3.2 introduces the Morse–Witten model.

In addition to the repulsive contact forces, each bubble also experiences an attractive radial force towards the axis of the liquid-filled rotating cylinder in which it is confined. For a bubble of volume V, with its centre at distance r from the axis of rotation, the magnitude F of this centripetal force is $F = kr$, with force constant k given by $k = V\Delta\rho\omega^2$. Here $\Delta\rho$ is the density difference between bubble and liquid, and ω is the angular frequency of the rotation.

3.1. Soft spheres

Our soft sphere simulations follow the approach by Winkelmann *et al.* who studied chains of soft spheres in a cylindrically symmetric confining potential, as defined above, for a limited range of compression [21]. In contrast to the dynamic simulations by [13], involving forces due to both inertia and viscous drag, this much simpler static model includes only repulsive harmonic (Hookean) forces, resulting from sphere overlaps. When applied to the case of contacting bubbles with surface tension γ, the Hookean force constant k_b is typically set to $k_b = \gamma/2$, in analogy to a system of two springs in series, each with spring constant γ [20]. At the end points of the chain, at $z = 0$ and $z = L$, the spheres are confined by hard walls (again leading to a repulsive Hookean force).

The total energy of the system is the sum of the energy due to the overlap between spheres and that due to the transverse harmonic confining potential, which varies quadratically with the distance of a sphere centre from the axis of rotation as in [21]. The structure of minimum energy (for given number and diameter of spheres, and length L) is obtained from an energy minimisation using gradient descent.

We have carried out a detailed set of simulations for a fixed number of soft spheres, $N = 10$ and for a specified value of k/k_b, representing the ratio of confinement strength to the strength of sphere repulsion. Starting from a length $L = 10$, at which all bubbles (of diameter 1) are aligned to form a straight linear chain, we decrease L in small steps of $\Delta L = 0.001$, and iteratively compute the minimum energy structure at each step.

The types of structures that we find include those seen in the experiments described in Section 2 for higher N. In addition to these we find a number of non-planar arrangements which are known also from dense packings of hard spheres in cylinders [22]. Table 1 shows all structures, together with alternative forms of notation. We have also listed the number of contacts of a sphere placed in the middle section of the respective chain.

We have repeated such calculations for a range of values of k/k_b; all data is presented in the stability diagram shown in Figure 3(a), discussed in Section 3.3.

Table 1. Table of the structures considered here. The images are taken from Morse-Witten simulations (Section 3.2) of 10 bubbles, placed between two parallel hard walls, with non-dimensional ratio $k/\gamma = 0.4$ (defined in Section 3), except for that of the twisted zipper, which is from a soft sphere simulation (Section 3.1) for $k/k_b = 0.1$.

Structure	Primary notation	Phyllotactic notation	Names	Number of contacts of a sphere (in middle section)
	Straight chain	1-1-0	Bamboo, linear chain	2
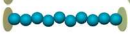	Buckled chain [planar]		Modulated zig–zag	2
	Doublet [planar]			3
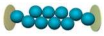	Zipper [planar]	2-1-1	Uniform zig–zag, girder	4
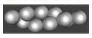	Twisted Zipper [planar]	2-$\underline{1}$-1	Twisted zig–zag	4
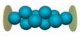 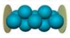	Tetrahedral structure (A,B)[non-planar]	2-2-0		5
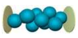	Three spiral structure [non-planar]	3-2-1	Boerdijk–Coxeter helix Bernal spiral, tetrahelices	6
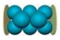	Four pillar structure [non-planar]	4-2-2		6
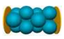	Layered triangular [non-planar], for $N =$ 12	3-3-0		6

3.2. Simulations using the Morse–Witten model for bubbles

While the soft sphere model introduced above is a convenient tool for simulating aggregates of soft spheres, it does not have any systematic theoretical justification. This is different for the model developed by Morse and Witten [15, 16] which is based on a linearisation of the Young–Laplace equation, representing the balance of the force due to surface tension and the pressure difference across a liquid interface. Its key features are two-fold in the present case. Firstly, the compressive force acting between two bubbles is softer than harmonic due to the presence of a logarithmic term. Secondly, applied to a bubble with multiple contacts, the theory results in (non-local) many-body forces, as a consequence of the deformability of the bubble. Bubble–bubble interactions are not pairwise-additive [23, 25].

In the following we consider chains of N equal-volume bubbles in confinement. For given boundary conditions (i.e. chain length and ratio k/γ of confinement strenght to surface tension), the system is described by the coordinates of the N bubble centres, and those of all the contacts that bubbles make with either other bubbles or the hard walls at both ends of the chain.

The Morse–Witten theory provides an expression for the (radial) displacement x_{mi} of the surface of bubble m at a given contact with bubble i which depends on both magnitudes and directions of the forces f_{mj} acting at *all* contacts of bubble m. We define displacement x_{mi} as the difference between the distance of the centre of mass of bubble m to the contact point, and its radius R, when undeformed. Expressed in dimensionless units (distances are normalised

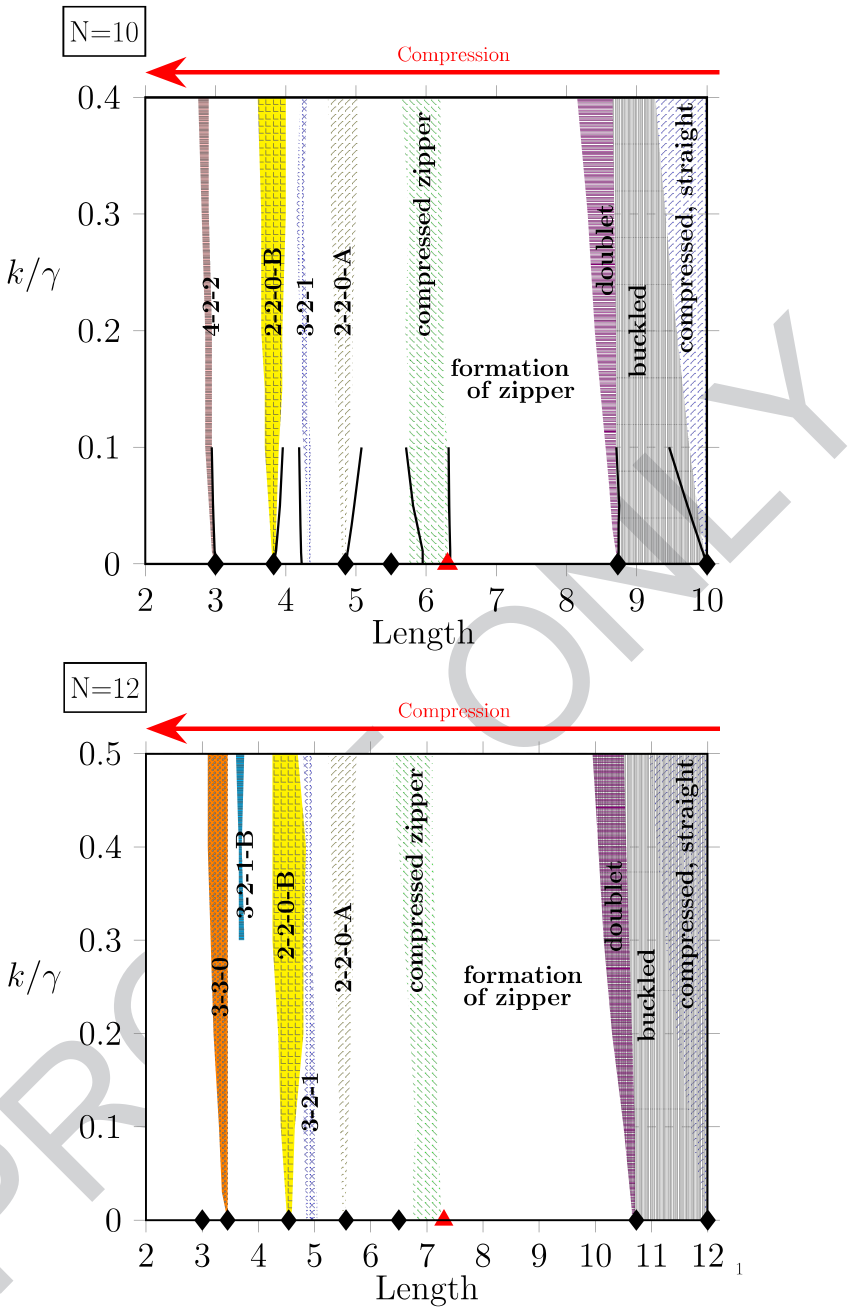

Colour online, B/W in print

Figure 3. Stability diagrams computed using the Morse–Witten model, for chains of $N = 10$ and $N = 12$ bubbles, respectively. The chains, whose lengths are expressed in multiples of the bubble diameter, are compressed between two hard walls, placed at either ends. The diagrams are computed for increasing compression, and fixed values of the ratio k/γ, of the force constant k of the harmonic confining potential and surface tension γ. The coloured regions correspond to homogeneous structures, with non-homogeneous structures left in white. The black lines in the diagram for $N = 10$ and $k/\gamma < 0.1$ are from soft sphere simulations (Section 3.1), with γ set to $k_b/2$ [20]. The black diamonds and red triangles mark the analytical results obtained for hard sphere packings; see Appendix 1.

by R, forces are normalised by γR), it is given by [16, 23]

$$x_{mi} = \frac{1}{24\pi}\left[5 + 6\ln\left(\frac{f_{mi}}{8\pi}\right)\right] - \sum_{j\neq i} G(\theta_{i(m)j(m)})f_{mj}. \tag{1}$$

Here, f_{mj} is the force at the contact of bubble m with bubble j or a hard wall. $\theta_{i(m)j(m)}$ is the angle between vectors pointing from the origin to contacts i and j of bubble m. The function $G(\theta)$ is given by [15, 16]

$$G(\theta) = -\frac{1}{4\pi}\left\{\frac{1}{2} + \frac{4}{3}\cos\theta + \cos\theta\ln\left[\sin^2(\theta/2)\right]\right\}. \tag{2}$$

To implement the force law, Equation (1), in an iterative computer simulation we proceed as follows. Our variables are the coordinates of the N bubble centres, and those of all bubble contact points. We consider a system to be in equilibrium when the net force acting on a bubble is zero (in practice some threshold value), and when the forces acting at each contact are consistent, i.e. $f_{mi} = f_{im}$ for all i, m; see the discussion below.

Initial values for the displacements at contacts, x_{mi}, are obtained from the overlap of bubbles that are approximated as spheres. Computation of the corresponding forces f_{mi} requires an inversion of the nonlinear Equation (1). This is achieved numerically using Powell's dog leg method [26, 27], as is implemented in a SciPy Python library. Each bubble centre is then moved in the direction of, and in proportion to, the net force acting on it; here the net force is the sum over all the forces acting on its contacts, together with the force due to the confining potential. To prevent oscillations near the equilibrium, we introduce some damping.

The movement of bubble centres may lead to the creation or loss of points of contact. We check for this only along the centre–centre lines of nearby bubbles; this is a simplification which is approximately valid for small forces, resulting in bubbles that remain almost spherical.

In addition to the condition of mechanical equilibrium of the bubble centres it is also necessary to ensure that Newton's Third Law is obeyed at the contact points, i.e. $f_{mi} = f_{im}$, since this is not enforced by Equation (1). The non-pairwise nature of the Morse–Witten interaction implies that a contact point is not necessarily at the midpoint of the centre–centre line between contacting bubbles m and i, with their centres located, respectively, at $\vec{Y}_m$ and $\vec{Y}_i$. It is rather at $p\vec{Y}_m + (1-p)\vec{Y}_i$, for a value of the parameter p between 0 and 1. A new contact is initiated with $p = 0.5$, i.e. at the midpoint. After the forces f_{mi} are determined for each bubble, the forces acting on either side of a given contact point are compared. The contact point is then moved in the direction proportional to the force difference $f_{mi} - f_{im}$ in order to minimise this difference, and so the parameter p deviates from 0.5 throughout the simulation. The procedure is different when dealing with bubble–wall contacts. In this case, the contact point is given the same radial coordinate as the bubble and the force due to the wall contact acts in the direction normal to the wall.

Using the updated positions of the bubble centres and contact points we sum up the net forces acting on all the bubbles. We consider the system equilibrated when the magnitude of the sum falls below a pre-defined threshold value (usually taken as 10^{-8} everywhere). If this is not the case, then each bubble centre is moved in the direction of the net force acting on it to start a further iteration.

An equilibrated configuration is then taken as the starting configuration for equilibration at slightly higher compression, obtained by reducing the distance between the hard walls. The change in compression due to the new position of the hard walls is experienced at first by the outermost bubbles.

The Morse–Witten model also provides an analytical expression for the deformation of a bubble due to a contact. Since the theory is linear, solutions for the displacement profiles, obtained for the case of several contacts, acted upon by forces, can be simply added. Examples of computed structures for $N = 10$ and dimensionless force constant ratio $k/\gamma = 0.4$ are shown in Table 1. Figure 2 shows two 12-bubble structures at a higher value of $k/\gamma = 0.75$, resulting in a larger deviation from sphericity of the bubble shapes.

We have systematically explored the sequences of structural transitions obtained upon compressing an initially straight chain by performing simulations for $N = 10$ and $N = 12$ bubbles. For each run, the ratio of spring constant of the confining potential k and surface tension γ was fixed. The simulation results are displayed in Figure 3. For $N = 10$ we also show the data obtained using the soft sphere model described in Section 3.1, for $k_b = \gamma/2$.

3.3. Stability diagrams

Two examples of stability diagrams are shown in Figure 3. All data was obtained by starting the simulations from a straight chain, and shortening this sequentially by not more than five percent of a bubble diameter, keeping the dimensionless ratio k/γ (representing the balance of attractive confining force and repulsive contact forces) constant.

Following equilibration, the type of structure obtained was determined from both visual inspection and examination of the number of contacts of each bubble. We recognise homogeneous structures in which all bubbles, except the ones in contact with a hard wall, are in the same environment. The corresponding regions in which these are found in the stability diagram are displayed in colour; regions that feature non-homogeneous structures are shown in white.

For hard spheres, i.e. the limit of $k/\gamma = 0$, exact expressions exist for the length of the various homogeneous structures for given N; see Appendix 1. We have evaluated these for $N = 10$ and $N = 12$ and marked them in Figure 3.

A linear chain made up of hard spheres buckles under an infinitesimal compression [14], but for finite values of k/γ the chain remains straight, as the shortening of the chain can be accommodated by a change of shape of the bubbles until k/γ reaches a critical value. The buckled phase takes the form of a modulated zig-zag pattern of transverse bubble displacements, with a maximum in the middle of the chain (see Figure 1). It is at the vicinity of this maximum that additional contacts are formed for a critical value of compression, resulting in a doublet. Further compression lead to the accumulation of such doublets in a process which reminds us of the closing of a 'zipper' [18]. We consider a closed zipper as fully formed once all but the two end bubbles have formed their additional contacts.

A further shortening of the chain maintains, but compresses this structure ('compressed zipper'), until at some critical value of compression, starting at each end, the zipper begins to transform into a 3d (i.e. non-planar) configuration. It is at this stage that the results of the soft sphere simulations of Section 3.1 differ qualitatively from those obtained using the Morse–Witten theory, as described in Section 3.2. The soft sphere simulations show a twisting of the zipper structure, similarly to that in the experiments shown in Figure 1; this is not seen in the Morse–Witten simulations, which show a gradual transformation of the compressed zipper into the tetrahedral structure 2-2-0-A. Any twist that we artificially introduce into the zipper eventually disappears, over the course of iteration to equilibrium. In the experiments described in Section 2, friction between contacting spheres may play a role in stabilising the twisted structure.

The 2-2-0-A structure is observed over a range of values of compression before a further increase leads to a gradual transition into the three-spiral structure 3-2-1. Further compression recovers the tetrahedral arrangement, but now the two bubbles at the end also adhere to it. We call this the 2-2-0-B structure (see Figure 1).

While the above scenario was found to be the same for $N = 10$ and $N = 12$, different transitions are observed upon further compression. For $N = 10$ the 2-2-0-B structure morphs into the four-pillar structure 4-2-2. Interestingly, for $N = 12$ the type of transition depends on the value of k/λ. For values $k/\lambda \lessapprox 0.3$, we observe a transition to 3-3-0, i.e. a structure made up of interlocked sub-units of three bubbles (layered triangular structure, see Table 1). Values $k/\lambda \gtrsim 0.3$ result in a transition back to the three-spiral structure, but with different positions of the end bubbles, we label this 3-2-1-B. Further compression leads to the 3-3-0 structure. This structure is quite stable and prevents the formation of the four-pillar structure 4-2-2 which we see for $N = 10$.

Winkelmann *et al.* [21] used a different approach to the study of packings of soft spheres in a harmonic transverse confining potential, valid in the limit $N \to \infty$. It takes as its starting point maximal-density packings of hard spheres in cylinders. A rotational energy can be associated with each of these, based on the distance of the corresponding sphere centres from the cylindrical axis. Packings of soft spheres were obtained by allowing for sphere overlaps (for the given structure), leading to the contribution of an overlap energy to the total energy. Structures of minimal energy were then computed via energy minimisation with respect to the distance of bubble centres to the axis, and with respect to a possible twist angle [21]. From these data, a phase diagram was constructed which indicates the structure of the lowest energy for a given value of compression and ratio k/k_b of the force constants for confinement and overlap in the soft sphere model. That diagram, Figure 3 in [21], is in broad agreement with our findings for $N = 10$ and $N = 12$, in the range of compression where both studies overlap. The key differences are as follows. The transition from 2-1-1 (zipper) to 2-2-0 occurs via a binary mixture of both structures, i.e. there is no twisted zipper (2-$\underline{1}$-1). In the limit $N \to \infty$, the structures 2-2-0-A and 2-2-0-B are identical, as are 3-2-1 and 3-2-1-B. The 3-3-0 structure only exists up to $k/k_B = k/(\gamma/2) \simeq 0.5$, where it vanishes in a peritectoid point [21]. There is also a region where there is a binary mixture of 3-3-0 and 4-2-2, unlike what we observe in our simulations for finite N.

4. Summary and outlook

We have presented a detailed computational study of the structural transitions that are encountered when an initially linear chain of bubbles, placed in a cylindrically symmetric confining potential, is compressed. The results were summarised in stability diagrams, computed for 10 and 12 bubbles, respectively. Different types of finite-size effects can be identified. They can be related to a mismatch of the periodicity of a structure with the total number of bubbles, or to the role of the bubbles at each end. For spheres, future experiments could further explore this role by having the two end spheres glued, slightly off-centre, onto the two stoppers. This might act as a template for obtaining strained or chiral structures. Using stoppers with a slanted flat surface, attached with different orientations at both ends, could play a similar role, suitable also for experiments with bubbles.

We have simulated structure formation by implementing the Morse–Witten theory for bubbles, exact in the limit of hard spheres. Only very limited use has been made of this theory in the past, either in 2D [29], or 3D [23, 25, 30]. We have developed an algorithm which allows for its use in a wider context than presented here. Instead of having a harmonic confining potential, as in our current simulations, one could for example introduce a cylindrical hard wall boundary to confine the bubbles. This would allow for the simulation of columns of *wet* 3d foams [31] or emulsions. Furthermore it is possible to add gravity to such simulations, so that a bubble experiences the weight of the bubbles placed above it. This effect is responsible for the observation of structural transitions in long columns of foam, and also in columns of hydrogels, as seen in the experiments by Irannezhad *et al.* [2].

Finally, we note that our observed self-assembly of particles into ordered arrangements due to the presence of confining forces is a common phenomenon in nature. This includes packings of seeds in pomegranates, clusters of ions in a confining electric field [32, 33], or floating magnets in magnetic confinement [34, 35]. Recent results for various soft matter systems are to be found in [36].

Acknowledgments

We thank Aleksander Prymek for incorporating the Blender visualisation software in the Python code for the Morse–Witten simulations. **A.M.**, **D.W.** and **S.H.** would like to thank the Isaac Newton Institute for Mathematical Sciences for support and hospitality during the programme 'GeomPack: Geometry and packing in material structure and biology' when some of the work on this paper was undertaken.

Disclosure statement

Q4 No potential conflict of interest was reported by the author(s).

Funding

Q5 **S.H.** and **J.R.-P.** were supported by the European Space Agency SciSpacE program (project 'REFOAM', contract number 4000129502/20/NL/PG). **A.I.** acknowledges funding from the Trinity College Dublin Provost's PhD Project Awards. **M.W.** acknowledges SURE-2023 Internship funding from the School of Physics, TCD. **A.M.** Acknowledges funding from
Q6 Trinity College Dublin through the Visiting Professor Fund.

ORCID

A. Irannezhad http://orcid.org/0000-0002-7297-2023
A. Mughal http://orcid.org/0000-0002-8738-9818

References

[1] J. Winkelmann and H.-K. Chan, Columnar Structures of Spheres: Fundamentals and Applications, CRC Press, 2023.

[2] A. Irannezhad, A. Baragry, D. Weaire, A. Mughal, and S. Hutzler, *Packing soft spheres: Experimental demonstrations with hydrogels*, Eur. J. Phys. 44(6) (2023), pp. 065501.

[3] J. Norman, E.L. Sorrell, Y. Hu, V. Siripurapu, J. Garcia, J. Bagwell, P. Charbonneau, S.R. Lubkin, and M. Bagnat, *Tissue self-organization underlies morphogenesis of the notochord*, Philos. Trans. R. Soc. B: Biolog. Sci. 373(1759) (2018), pp. 20170320.

[4] L. Fu, C. Bian, C.W. Shields IV, D.F. Cruz, G.P. López, and P. Charbonneau, *Assembly of hard spheres in a cylinder: A computational and experimental study*, Soft Matter. 13(18) (2017), pp. 3296–3306.

[5] T. Liu, H.-K. Chan, and D. Wan, *Chiral photonic crystals from sphere packing*, Soft Matter. 19(38) (2023), pp. 7313–7322.

[6] S.N. Fejer, D. Chakrabarti, H. Kusumaatmaja, and D.J. Wales, *Design principles for Bernal spirals and helices with tunable pitch*, Nanoscale. 6(16) (2014), pp. 9448–9456.
[7] M.S. Fernández, V.R. Misko, and F.M. Peeters, *Self-assembly of Janus particles into helices with tunable pitch*, Phys. Rev. E. 92(4) (2015), pp. 042309.
[8] A.H. Boerdijk, *Some remarks concerning close-packing of equal spheres*, Philips Res. Rep. 7 (1952), pp. 303–313.
[9] H.S.M. Coxeter, Regular Complex Polytopes, 1st ed., Cambridge University Press, 1974.
[10] J.D. Bernal, *Geometry of the structure of monatomic liquids*, Nature. 185(4706) (1960), pp. 68–70.
[11] J.D. Bernal, *The Bakerian lecture, 1962. The structure of liquids*, Proc. R. Soc. Lond. A. Math. Phys. Sci.280(1382) (1964), pp. 299–322.
[12] J.F. Sadoc and N. Rivier, *Boerdijk–Coxeter helix and biological helices*, Eur. Phys. J. B: Condens. Matter Complex Syst. 12(2) (1999), pp. 309–318.
[13] T. Lee, K. Gizynski, and B.A. Grzybowski, *Non-equilibrium self-assembly of monocomponent and multicomponent tubular structures in rotating fluids*, Adv. Mater. 29(47) (2017), pp. 1704274.
[14] S. Hutzler, J. Ryan-Purcell, A. Mughal, and D. Weaire, *A continuum description of the buckling of a line of spheres in a transverse harmonic confining potential*, R. Soc. Open. Sci. 10(7) (2023), pp. 230293.
[15] D.C. Morse and T.A. Witten, *Droplet elasticity in weakly compressed emulsions*, Europhys. Lett. 22(7) (1993), pp. 549–555.
[16] R. Höhler and D. Weaire, *Can liquid foams and emulsions be modeled as packings of soft elastic particles?* Adv. Colloid Interface Sci. 263 (2019), pp. 19–37.
[17] Redhill Precision Specialty Balls, Polypropylene balls (pp). Available at https://www.redhillballs.com/.
[18] A. Irannezhad, D. Weaire, A. Mughal, J. Ryan-Purcell, and S Hutzler, *Buckling of a tilted line of confined hard spheres*, Philos. Mag. 102(24) (2022), pp. 2506–2524.
[19] M. van Hecke, *Jamming of soft particles: Geometry, mechanics, scaling and isostaticity*, J. Phys: Condens. Matter. 22(3) (2009), pp. 033101.
[20] D.J. Durian, *Bubble-scale model of foam mechanics: Mmelting, nonlinear behavior, and avalanches*, Phys. Rev. E. 55(2) (1997), pp. 1739.
[21] J. Winkelmann, A. Mughal, D.B. Williams, D. Weaire, and S. Hutzler, *Theory of rotational columnar structures of soft spheres*, Phys. Rev. E. 99(2) (2019), pp. 020602.
[22] A. Mughal, H.K. Chan, D. Weaire, and S. Hutzler, *Dense packings of spheres in cylinders: Simulations*, Phys. Rev. E. 85(5) (2012), pp. 051305.
[23] R. Höhler and S. Cohen-Addad, *Many-body interactions in soft jammed materials*, Soft
Q7 Matter. 13(7) (2017), pp. 1371–1383.
[24] R. Höhler and S. Cohen-Addad, *Many-body interactions in soft jammed materials*, Soft Matter. 13(7) (2017), pp. 1371–1383.
[25] G. Ginot, R. Höhler, S. Mariot, A.M. Kraynik, and W. Drenckhan, *Juggling bubbles in square capillaries: An experimental proof of non-pairwise bubble interactions*, Soft Matter. 15(22) (2019), pp. 4570–4582.
[26] M.J.D. Powell, A hybrid method for nonlinear equations, in *Numerical Methods for Nonlinear Algebraic Equations*, P. Robinowitz, ed., Gordon and Breach, 1970, pp. 87–161.
[27] M.J.D. Powell, A new algorithm for unconstrained optimization, in *Nonlinear Programming*, J.B. Rosen, O.L. Mangasarian and K. Ritter, eds. Elsevier, 1970, pp. 31–65.
[28] Available at https://www.blender.org/.
[29] F.F. Dunne, J. Winkelmann, D. Weaire, and S. Hutzler, *Implementation of Morse–Witten theory for a polydisperse wet 2D foam simulation*, Philos. Mag. 99(18) (2019), pp. 2303–2320.

[30] S. Hutzler, F.F. Dunne, A.M. Kraynik, and D. Weaire, *The energy of fcc and hcp foams*, Soft Matter. 16(35) (2020), pp. 8262–8271.

[31] A.J. Meagher, F. García-Moreno, J. Banhart, A. Mughal, and S. Hutzler, *An experimental study of columnar crystals using monodisperse microbubbles*, Colloids Surf. A: Physicochem. Eng. Aspects. 473 (2015), pp. 55–59.

[32] R.C. Thompson, *Ion coulomb crystals*, Contemp. Phys. 56(1) (2015), pp. 63–79.

[33] A. Mughal, S. Hutzler, and D. Weaire, *Equilibrium states of confined ions in two dimensions*, Philos. Mag. 103(6) (2023), pp. 595–609.

[34] I.V. Nemoianu, C.G. Dragomirescu, V. Manescu, M.-I. Dascalu, G. Paltanea, and R.M. Ciuceanu, *Self-organizing equilibrium patterns of multiple permanent magnets floating freely under the action of a central attractive magnetic force*, Symmetry. 14(4) (2022), pp. 795.

[35] P.D.S. de Lima, A. Lyons, A. Irannezhad, J.M. de Araújo, S. Hutzler, and M.S. Ferreira, *Self-assembled clusters of magnetically tilted dipoles*, preprint (2024), submitted for publication.

[36] H.-K. Chan, S. Hutzler, A. Mughal, C. O'Hern, Y. Wang, and D. Weaire*Packing Problems in Soft Matter Physics*, Royal Society of Chemistry, 2025, forthcoming

Appendix 1. Analytical results for hard sphere structures in confinement

For hard sphere packings, the lengths of the uniform structures discussed in the main text can be computed from geometrical considerations. Table A1 summarises the results.

They are in good agreement with our simulation data for $N = 10$ and $N = 12$, in the hard sphere limit $k/\gamma \to 0$; see Figure 3. Only our value for the length of the Boerdijk–Coxeter structure does not match the data; presumably due to some end effect.

In the limit of $N \to \infty$, all our analytical results match the findings by Winkelmann *et al.* in the hard sphere limit [21].

Table A1. Analytical expressions for the length of chains of *hard* spheres, arranged in various structures. For simplicity, we restrict ourselves to an even number of spheres, N. The result for 3-3-0 is valid for $N \bmod 3 = 0$. 'Full' zipper refers to a uniform arrangement. We find that in our simulations the spheres at both ends of the chain are not part of the zipper arrangement. In our tabulated expression, we correct for this end effect by placing these two spheres on the cylinder axis. (The function floor(x) denotes the greatest integer number which is less or equal to x.)

Structure	Length/Diameter, L/D	L/D ($N = 10$)	L/D ($N = 12$)	L/(ND), $N \to \infty$
Doublet	$1 + \sqrt{3} + (N - 4)$	8.73	10.73	1
Full zipper with end correction	$\frac{1}{2}(\sqrt{13} - 1 + N)$	6.30	7.30	$\frac{1}{2}$
Full zipper	$\frac{1}{2}(1 + N)$	5.50	6.50	$\frac{1}{2}$
2-2-0-A	$1 + \sqrt{3} - \sqrt{2} + N/(2\sqrt{2})$	4.85	5.56	$1/(2\sqrt{2}) \simeq 0.35$
3-2-1 (Boerdijk–Coxeter)	$1 + (N - 1)/\sqrt{10}$	3.85	4.48	$1/\sqrt{10} \simeq 0.32$
2-2-0-B	$1 - 1/\sqrt{2} + N/(2\sqrt{2})$	3.83	4.54	$1/(2\sqrt{2}) = 0.354$
3-3-0	$1 + \sqrt{\frac{2}{3}}(N/3 - 1)$	*N/A*	3.45	$\sqrt{\frac{2}{3}}/3 \simeq 0.27$
4-2-2	$1 + \frac{1}{2}\text{floor}((N - 1)/2)$	3	3.5	1/4